JOURNAL OF SOLID STATE CHEMISTRY 22, 157–170 (1977)

The Crystal Chemistry of the M^+VO_3 (M^+ = Li, Na, K, NH_4, Tl, Rb, and Cs) Pyroxenes

F. C. HAWTHORNE

Department of Earth Sciences, University of Manitoba, Winnipeg, Manitoba, Canada R3T 2N2

AND

C. CALVO*

Department of Chemistry, McMaster University, Hamilton, Ontario, Canada L8S 4M1

Received February 15, 1977; in final form April 21, 1977

The crystal structures of M^+VO_3(M^+ = K, NH_4, Rb, and Cs) have been refined using three-dimensional counter–diffractometer X-ray data and full-matrix least-squares methods. The structure of these compounds is characterized by a $(V^{5+}O_3^{2-})_\infty^-$ chain extending along the *c*-axis (*Pbcm* orientation), with adjacent chains linked by the alkali metal cation. The structure may be considered as a variant of the pyroxene structure, and standard atom nomenclature is proposed in order to facilitate comparison with silicate pyroxenes. Structural variation across this series is discussed in detail and is compared with the analogous $M^+M^{3+}Si_2O_6$ (M^+ = Li, Na; M^{3+} = Al, Cr, Fe, Sc, In) series.

Introduction

The pyroxene structure is one of extreme flexibility and a wide variety of compounds crystallize in one or more variants of this structure type. Although the basic structure has been known for many years (*1*), it is only recently that the diversity in structural variation has been recognized. Because of the importance of pyroxenes as rock-forming minerals, the silicate varieties have been extensively investigated (*2*, *3*). However, further insight into this structure type is available from the wide variety of nonsilicate pyroxenes, which show extremes of structural distortion and additional structural variants that are not present (or as yet discovered) in the silicate varieties. Recent studies (*4–7*) indicate that the tetrahedral oxyanion $(V^{5+}O_4^{2-})^{3-}$ is particularly responsive to changes in local environment. Thus the vanadate pyroxenes M^+VO_3 (M = Li, Na, K, NH_4^+, Rb, Cs, Tl) would appear to be particularly appropriate for a systematic examination of topological variation in a morphotropic pyroxene series.

The crystal structure of $NaVO_3$ was determined by Sørum (*8*) who showed that the structure was similar to that of diopside. Despite the suggestion by Feigelson, Martin, and Johnson (*9*) that Weissenberg photographs indicated that the space group could be *Cc* as well as *C*2/*c*, the *C*2/*c* structure has recently been confirmed by structure refinement (*10*, *11*). On the basis of cell dimensions and space group, several recent studies have assumed that $LiVO_3$ has the same structure

* Deceased.

ISSN 0022-4596

(*12*, *13*) and this has been confirmed by Shannon and Calvo (*14*). Different cell parameters were obtained for $LiVO_3$ by Feigelson, Martin, and Johnson (*9*), but these were later shown to be in error (*15*). Lukesh (*16*, *17*) showed that the structure of NH_4VO_3 was an orthorhombic pyroxene variant, and this was independently confirmed by Synecek and Hanic (*18*). The same structure was also found for KVO_3 (*19*, *20*) and structure refinements of both compounds were later reported by Evans (*21*). The crystal structures of $RbVO_3$ and $CsVO_3$ were solved by Calvo (*22*) who showed them to be isotypic with KVO_3. On the basis of space group and cell dimensions, this structure was also proposed for $TlVO_3$ (*23*) and this has recently been confirmed (*24*). As recent refinements are available only for $LiVO_3$, $NaVO_3$, and $TlVO_3$, the structures of KVO_3, NH_4VO_3, $RbVO_3$, and $CsVO_3$ are refined here to provide accurate parameters for a systematic examination of the structural variation in this series.

Collation and comparison of results would be greatly simplified by adoption of a consistent atomic nomenclature for the metavanadate structures, similar to those adopted by Megaw (*25*) for the feldspar structures and by Burnham, Clark, Papike, and Prewitt (*26*) for the silicate clinopyroxenes. The alkali metal coordination is completely different in the orthorhombic and monoclinic metavanadate structures; however, the single metavanadate chain is fairly similar in each

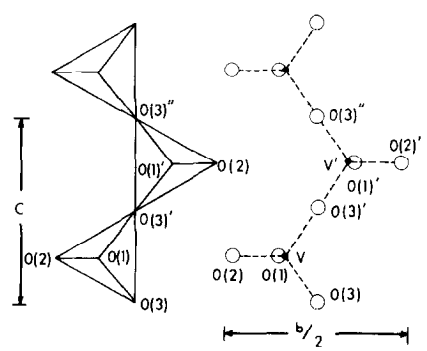

FIG. 1. Recommended atomic nomenclature for the alkali–metal metavanadates.

structure, and all the crystallographically unique anions are bonded to the vanadium. Thus the anions may be labeled with respect to their configuration in the chain; the proposed nomenclature is illustrated in Fig. 1. This is the same as that used by Shannon and Calvo (*14*) for $LiVO_3$ and Marumo, Isobe, and Iwai (*11*) for $NaVO_3$, but is different from the nomenclature previously used for the orthorhombic alkali metal metavanadates (*21*). This nomenclature also has the advantage of allowing direct comparison with the silicate clinopyroxens that have comparable metasilicate chains. With regard to the monoclinic metavanadates, the cation nomenclature used is that of Shannon and Calvo (*14*); thus for $NaVO_3$ (*11*), Na_I becomes Na(2) and Na_{II} becomes Na(1). This facilitates direct comparison of these sites with the corresponding $LiM^{3+}Si_2O_6$ clinopyroxenes (*27–32*).

Experimental

Crystals of ammonium metavanadate were grown by dissolving powdered NH_4VO_3 in water at 80°C and allowing the solution to cool to room temperature. Crystals of the other orthorhombic metavanadates were grown from a stoichiometric mixture of $M_2^+CO_3$ and V_2O_5 that was heated in a Pt crucible at 750°C for 4 hr, cooled to 300°C at 5°C/hr and allowed to cool to room temperature in the furnace. Single crystal precession photographs exhibited orthorhombic symmetry with systematic absences consistent with the space group *Pbcm*. The crystals were mounted on a Syntex $P\bar{1}$ automatic four-circle diffractometer using graphite monochromated Mo$K\alpha$ radiation (λ = 0.71069 Å) and a scintillation counter. Cell dimensions were determined by least-squares refinement of 15 automatically aligned reflections. Intensities were collected in the θ–2θ scan mode at variable rates from 2.0–24.0°/min depending on the peak count through an angle of 2° and the α_1–α_2 separation. Background counts were made at the beginning and end of each scan. A

TABLE I

CRYSTALLOGRAPHIC DATA FOR THE METAVANADATE PYROXENES

	$LiVO_3$	$NaVO_3$	KVO_3	NH_4VO_3	$RbVO_3$	$CsVO_3$	$TlVO_3$
a (Å)	10.158(2)	10.552(3)	5.176(2)	4.909(1)	5.261(1)	5.393(1)	5.16(1)
b (Å)	8.418(1)	9.468(2)	10.794(3)	11.786(2)	11.425(2)	12.249(2)	11.22(2)
c (Å)	5.885(1)	5.879(2)	5.680(2)	5.830(1)	5.715(1)	5.786(1)	5.73(1)
β (°)	110.48(2)	108.47(3)	—	—	—	—	—
V (Å^3)	471.4	557.1	317.3	337.3	343.5	382.2	331.8
Z	8	8	4	4	4	4	4
Space group	$C2/c$	$C2/c$	$Pbcm$	$Pbcm$	$Pbcm$	$Pbcm$	$Pbcm$
ρ_c	2.985	2.907	2.889	2.303	3.565	4.028	6.070
Reference	(*14*)	(*11*)	This study	This study	This study	This study	(*24*)

standard reflection was examined every 50 reflections to check on the crystal alignment; no significant variation was noted in any of the data collections. Reflections were collected over one asymmetric unit out to a 2θ value of 60°. Intensities were corrected for absorption, Lorentz, polarization, and background effects and were reduced to structure factors. A reflection was considered as observed if its magnitude exceeded that of three standard deviations based on counting statistics. The numbers of observed reflections for each crystal resulting from this procedure are given in Table II.

Crystal structure refinement was initiated with the positional parameters obtained in previous studies of these compounds. Initial refinement was performed using the full-matrix least-squares program CUDLS (*33*) and the final stages were accomplished using the program RFINE (*34*). Scattering factors for neutral atoms were taken from Cromer and Mann (*35*) with anomalous dispersion corrections from Cromer and Liberman (*36*). Refinement of all variables for an isotropic thermal model resulted in R factors (*37*) given in Table II. At this stage, the temperature factors were converted to anisotropic of the form

$$\exp\left(-\sum_{i=1}^{3}\sum_{j=1}^{3} h_i h_j \beta_{ij}\right),$$

and a correction was applied for extinction with the extinction coefficient included as a variable in the refinement (*38*). Full-matrix refinement of all variables resulted in convergence at R factors given in Table II. In the

TABLE II

SUMMARY OF CRYSTAL STRUCTURE REFINEMENTS

	KVO_3	NH_4VO_3	$RbVO_3$	$CsVO_3$
Total no. of unique reflections	587	642	604	532
No. of observed reflections	475	569	460	487
R^a (observed)%	6.8	5.9	7.2	5.1
R^a (all data)%	8.7	6.7	9.6	5.6
$R_w{}^a$ (observed)%	7.2	6.2	8.1	6.0
$R_w{}^a$ (all data)%	9.1	6.9	9.8	6.3
R^b (observed)%	5.6	4.5	4.9	3.0
R^b (all data)%	7.4	5.4	7.0	3.3
$R_w{}^b$ (observed)%	5.6	5.0	5.8	4.6
$R_w{}^b$ (all data)%	6.9	5.8	7.6	4.7

[a] Isotropic temperature factors.

[b] Anisotropic temperature factors.

TABLE IV

FINAL ATOMIC POSITIONS AND ANISOTROPIC TEMPERATURE FACTORS FOR $M^{+}VO_3$ (M = K, NH_4, Rb, Cs)

	x	y	z	U_{11}[b]	U_{22}	U_{33}	U_{12}	U_{13}	U_{23}
K	0.9357(4)	0.3954(2)	¼	267(9)	189(6)	294(10)	−62(6)	0	0
V	0.4765(3)	0.1617(1)	¼	136(5)	136(6)	64(5)	8(6)	0	0
O(1)	0.1602(11)	0.1486(6)	¼	166(27)	272(35)	260(31)	−25(25)	0	0
O(2)	0.6107(12)	0.0241(6)	¼	266(31)	153(24)	245(29)	59(25)	0	0
O(3)	0.5888(11)	¼	0	227(29)	212(24)	108(23)	0	0	31(10)
N	0.9371(11)	0.4128(4)	¼	B_{equiv} = 1.98(4) Å²					
V	0.4643(2)	0.17438(7)	¼	153(14)	127(7)	114(3)	0(3)	0	0
O(1)	0.1305(8)	0.1693(4)	¼	170(16)	274(21)	351(21)	41(3)	0	0
O(2)	0.5758(8)	0.0426(3)	¼	212(18)	162(14)	325(21)	50(5)	0	0
O(3)	0.5816(8)	¼	0	251(17)	239(14)	172(15)	0	0	45(14)
H(1)	0.790(16)	0.446(6)	¼						
H(2)	0.084(16)	0.464(6)	¼	B_{equiv}[a] = 1.5 Å²					
H(3)	−0.054(10)	0.371(4)	0.394(9)						
Rb	0.9305(2)	0.3981(1)	¼	276(6)	225(7)	334(7)	−55(3)	0	0
V	0.4660(3)	0.1661(1)	¼	158(7)	185(7)	180(8)	9(6)	0	0
O(1)	0.1568(15)	0.1495(7)	¼	201(32)	357(46)	319(48)	9(33)	0	0
O(2)	0.6022(15)	0.0385(7)	¼	245(38)	278(40)	361(46)	0(33)	0	0
O(3)	0.5682(14)	¼	0	286(34)	298(33)	244(33)	0	0	53(30)
Cs	0.9183(2)	0.4010(1)	¼	308(4)	251(8)	265(5)	−44(3)	0	0
V	0.4511(4)	0.1723(2)	¼	206(9)	213(8)	170(12)	3(7)	0	0
O(1)	0.1512(17)	0.1541(9)	¼	292(40)	295(53)	365(71)	−30(40)	0	0
O(2)	0.5901(19)	0.0533(7)	¼	367(52)	205(46)	378(68)	27(4)	0	0
O(3)	0.5455(16)	¼	0	330(46)	304(38)	220(51)	0	0	43(32)

[a] Not refined.

[b] Calculated from $\beta_{ij} = 2\pi^2 b_i b_j U_{ij}$ where b_i are the reciprocal lattice vectors and $U_{ij} = U_{ij} \times 10^4$.

TABLE V

INTERATOMIC DISTANCES (Å) AND ANGLES (°) IN THE ALKALI METAVANADATES

		KVO_3	NH_4VO_3	$RbVO_3$	$CsVO_3$	$TlVO_3$[a]
V–O(1)		1.643(6)	1.640(4)	1.638(8)	1.633(9)	1.61(3)
V–O(2)		1.639(6)	1.647(4)	1.625(8)	1.640(9)	1.62(3)
V–O(3)	×2	1.806(2)	1.803(1)	1.803(3)	1.805(3)	1.79(1)
O(1)–O(2)		2.691(9)	2.648(5)	2.664(11)	2.669(12)	2.66(4)
O(1)–O(3)	×2	2.853(7)	2.816(4)	2.836(9)	2.827(9)	2.78(3)
O(2)–O(3)	×2	2.824(5)	2.846(3)	2.813(7)	2.821(8)	2.80(2)
O(3)–O(3)*a*		2.840(1)	2.915(1)	2.858(1)	2.893(1)	2.865(5)
O(1)–V–O(2)		110.1(3)	107.3(1)	109.5(4)	109.3(5)	107(2)
O(1)–V–O(3)	×2	111.5(2)	109.7(1)	111.0(3)	110.6(3)	108(2)
O(2)–V–O(3)	×2	110.0(2)	111.1(1)	110.2(2)	109.9(2)	111(2)
O(3)–V–O(3)*a*		103.7(2)	107.9(1)	104.9(2)	106.6(2)	108(2)
M–O(1)*b*		2.778(7)	3.041(7)	2.909(8)	3.122(9)	2.93(3)
M–O(1)*c*		2.906(7)	3.023(7)	3.080(8)	3.275(9)	2.94(3)
M–O(1)*d*	×2	3.105(3)	3.215(3)	3.143(3)	3.225(4)	3.17(1)
M–O(2)*e*		2.728(7)	2.838(6)	2.936(8)	3.242(9)	2.94(3)
M–O(2)*f*		3.151(7)	2.946(2)	3.229(8)	3.316(9)	3.02(3)
M–O(2)*g*	×2	3.413(4)	3.452(3)	3.416(4)	3.437(6)	3.42(2)
M–O(3)	×2	2.775(4)	2.976(5)	2.922(5)	3.091(6)	2.88(2)
V–O(3)–V		142.5(4)	142.7(2)	145.3(5)	147.2(6)	145(2)

Equivalent positions: $a = x, y, \frac{1}{2} - z$; $b = -x, \frac{1}{2} + y, \frac{1}{2} - z$; $c = 1 + x, y, z$; $d = 1 + x, \frac{1}{2} - y, -z$; $e = 2 - x, \frac{1}{2} + y, \frac{1}{2} - z$; $f = 1 - x, y, \frac{1}{2} - z$; $g = x, \frac{1}{2} - y, -z$; $h = 1 - x, \frac{1}{2} + y, \frac{1}{2} - z$; $i = x - 1, \frac{1}{2} - y, \frac{1}{2} + z$; $j = x\ \frac{1}{2} - y, 1 - z$; $k = 1 + x, y, \frac{1}{2} - z$; $1 = -x, \frac{1}{2} + y, z$; $m = 2 - x, y - \frac{1}{2}, z$; $n = 1 - x, y - \frac{1}{2}, z$; $o = x - 1, y, z$; $p = x - 1, \frac{1}{2} - y, -z$.

[a] Data from (*24*).

TABLE VI[a]

INTERATOMIC DISTANCE (Å) AND ANGLES (°) AROUND NH_4 IN NH_4VO_3

N–H(1)		0.82(8)	H(1)–O(2)*h*	2.12(8)	
N–H(2)*c*		0.94(8)	H(2)–O(2)*h*	1.91(8)	
N–H(3)*c*	×2	0.97(5)	H(3)–O(3)*i*	2.37(5)	
⟨N–H⟩		0.93	H(3)–O(1)*j*	2.31(5)	
H(1)–H(2)*c*		1.46(9)	H(1)–N–H(2)*c*	111(6)	
H(1)–H(3)*c*		1.44(7)	H(1)–N–H(3)*c*	106(3)	
H(2)*c*–H(3)*c*		1.54(8)	H(2)*c*–N–H(3)*c*	107(3)	
H(3)*c*–H(3)*k*		1.68(9)	H(3)*c*–N–H(3)*k*	119(5)	
⟨H–H⟩		1.54	⟨H–N–H⟩	109.5	
N–O(1)*d*		3.215(3)	N–H(3)*c*–O(1)*d*	153(4)	
N–O(2)*e*		2.838(6)	N–H(2)*c*–O(2)*e*	169(6)	
N–O(2)*f*		2.946(6)	N–H(1)–O(2)*f*	176(7)	
N–O(3)		2.976(5)	N–H(3)*k*–O(3)	120(4)	

O(1)–V		1.640(4)	O(2)–V	1.647(4)	O)3)–V	×2	1.803(1)
O(1)–N1		3.041(7)	O(2)–N1	2.946(2)	O(3)–N	×2	2.976(5)
O(1)–N*o*		3.023(7)	O(2)–Nm	2.838(6)	O(3)–H(3)*k*	×2	2.37(5)
O(1)–N*p*	×2	3.215(3)	O(2)–N*g*	3.452(3)			
O(1)–H(3)*j*	×2	2.31(5)	O(2)–H(1)*n*	2.12(8)			
			O(2)–H(2)*n*	1.91(8)			

[a] Equivalent positions as in Table V.

TABLE VII

MAGNITUDES AND ORIENTATIONS OF THE PRINCIPAL AXES OF THE THERMAL ELLIPSOIDS

	rms displacement (Å²)	Angle to *a* axis	Angle to *b* axis	Angle to *c* axis
		KVO_3		
	0.125(3)	61(3)°	29(3)°	90°
K	0.171(3)	90	90	0
	0.174(3)	29(3)	119(3)	90
	0.080(3)	90	90	0
V	0.113(3)	139(12)	49(12)	90
	0.121(3)	49(12)	41(12)	90
	0.126(11)	13(12)	77(12)	90
O)1)	0.161(10)	90	90	0
	0.167(10)	103(12)	13(12)	90
	0.114(11)	114(8)	24(8)	90
O(2)	0.157(9)	90	90	0
	0.171(10)	24(8)	66(8)	90
	0.087(13)	90	116(7)	26(7)
O(3)	0.150(9)	0	90	90
	0.157(9)	90	26(7)	64(7)
		NH_4VO_3		
	0.107(2)	90	90	0
V	0.114(2)	93(7)	177(7)	90
	0.123(1)	3(7)	93(7)	90
	0.128(6)	11(7)	101(7)	90
O(1)	0.167(6)	101(7)	169(7)	90
	0.188(6)	90	90	0
	0.119(7)	61(8)	151(8)	90
O(2)	0.153(6)	151(8)	119(8)	90
	0.181(6)	90	90	0
	0.122(6)	90	117(7)	27(7)
O(3)	0.159(5)	0	90	90
	0.161(6)	90	27(7)	63(7)
		$RbVO_3$		
	0.138(2)	57(2)	33(2)	90
Rb	0.177(2)	147(2)	57(2)	90
	0.183(2)	90	90	0
	0.125(3)	19(10)	109(10)	90
V	0.134(3)	90	90	0
	0.137(3)	71(10)	19(10)	90
	0.142(12)	4(12)	94(12)	90
O(1)	0.179(13)	90	90	0
	0.189(12)	86(12)	4(12)	90
	0.156(12)	1(52)	91(52)	90
O(2)	0.168(11)	91(52)	179(52)	90
	0.190(12)	90	90	0
	0.113(14)	90	108(9)	18(9)
O(3)	0.169(10)	0	90	90
	0.177(10)	90	18(9)	72(9)
		$CsVO_3$		
	0.151(1)	61(2)	29(2)	90
Cs	0.163(2)	90	90	0
	0.182(1)	29(2)	119(2)	90
	0.130(5)	90	90	0
V	0.143(3)	158(33)	68(33)	90
	0.148(3)	68(33)	22(33)	90
	0.137(15)	8(11)	82(11)	90
O(1)	0.199(14)	82(11)	172(11)	90
	0.215(16)	90	90	0
	0.143(15)	100(14)	10(14)	90
O(2)	0.193(13)	170(14)	100(14)	90
	0.219(16)	90	90	0
	0.105(23)	90	102(10)	12(10)
O(3)	0.176(12)	90	168(10)	102(10)
	0.182(13)	0	90	90

final stages of the refinement of NH_4VO_3, difference Fourier maps in the vicinity of the NH_4^+ ion revealed small maxima in a tetrahedral arrangement around the N atom. These were inserted as H positions and refinement of all variables (with the exception of the H temperature factors which were fixed at 1.5 Å²) produced a reduction in the weighted R_w factor from 5.4 to 5.0%, an improvement that is significant at the 0.005 significance level (*39*). Observed and calculated structure factors from the final cycles of refinement are given in Table III.[1] Final atomic positions and anisotropic temperature factors are listed in Table IV. Interatomic distances and angles, and the magnitudes and orientations of the principal axes of the thermal ellipsoids were calculated with the program ERRORS (*34*) and are presented in Tables V, VI and VII.

Discussion

Two pyroxene structure types occur in the alkali metavanadates of the form M^+VO_3. Figure 2 shows a type I stability diagram (*40*) for this system. [8]-coordinate cation radii were used to construct this figure, with the exception of NH_4VO_3 where the [6]-coordinate radius was used. It has been shown (*50*) that for isostructural ammonium and potassium compounds, the coordination number of the NH_4^+ ion is always smaller than the coordination number of the K^+ ion despite the fact that the K^+ ion is significantly smaller than the NH_4^+ ion. This feature is apparent in the alkali-metal metavanadates where the K coordination number is [8] (or [10]) while the NH_4^+ ion coordination number is [6]. The division into two structural fields is immediately apparent. As expected, there is no

[1] Table III has been deposited as Document No. NAPS 03030 with the National Auxiliary Publications Service, c/o Microfiche Publications, 440 Park Avenue South, New York, New York 10006. A copy may be secured by citing the document number and by remitting $5.00 for photocopy or $1.50 for microfiche. Advance payment is required. Make check or money order payable to Microfiche Publications.

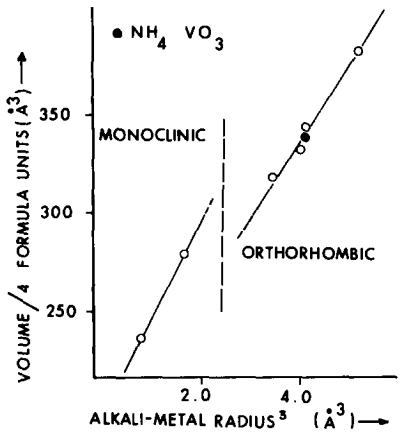

FIG. 2. Type I stability diagram for the alkali–metal metavanadates.

solid solution between neighboring compounds in different fields. However, double metavanadates do occur in this region; Perraud (*42*) showed that $NaK(VO_3)_2$ and $Na_3K(VO_3)_4$ occur as discrete phases in the system $NaVO_3$–KVO_3. The cell dimensions and space group for $NaK(VO_3)_2$ given by Perraud ($a = 5.80$, $b = 10.04$, $c = 10.54$, $\beta = 103.8°$; $C2/c$) suggest that the structure could be a pyroxene variant; the crystal structures for these two compounds have recently been solved (*49*), showing them both to be variants of the pyroxene structure.

The structures of $LiVO_3$ and $NaVO_3$ are illustrated in Fig. 3. Edge sharing chains of $M(1)$ octahedra extend in the c direction, and are linked by sharing corners to the infinite corner sharing chains of $V^{5+}O_4$ tetrahedra. Lying between the chains are the highly distorted $M(2)$ sites that provide additional linkage between the octahedral and tetrahedral chains. This produces a staggered layer motif; these are stacked (by the C-centering operation) on top of each other up the a axis to produce the overall structure. The structure of the orthorhombic metavanadates is shown in Fig. 4. As with the monoclinic phases, the structure is characterized by infinite tetrahedral chains. The alkali metal cation coordination is now [8] (or possibly [10]) and the octahedral chains of the monoclinic structure are replaced by edge-sharing chains of irregular [8]-coordinated polyhedra parallel to c. However, whereas the chains in the monoclinic structure are separated in the b–c plane by a double band of edge-sharing octahedra, the chains in the orthorhombic structure are separated by a single band of edge-sharing polyhedra. The stacking sequence is completely different from that in the monoclinic phases; Fig. 4b shows that successive layers of chains in the orthorhombic structure are

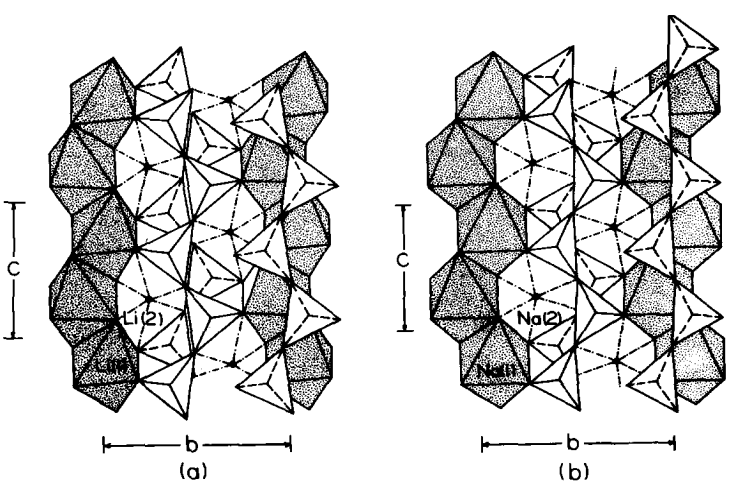

FIG. 3. The structures of the monoclinic alkali–metal vanadates, (a) $LiVO_3$, (b) $NaVO_3$, projected down the a axis.

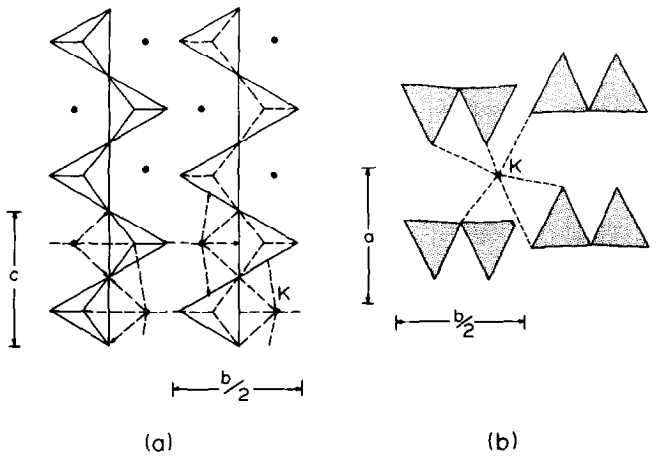

FIG. 4. The structure of the orthorhombic alkali–metal metavanadates (KVO_3): (a) projection down the a axis; those tetrahedra with full apical edges point along $+a$, those with broken apical edges point along $-a$. K–O bonds are indicated by broken lines; those bonds terminated by arrowheads connect to atoms removed by one a-axis translation from those shown in the figure. (b) projection along the c axis, showing the way in which the alkali–metal cation links adjacent $(V^{5+}O_3^{2-})_\infty^-$ chains.

repeated by a simple lattice translation whereas in the monoclinic structures, the layer is repeated by the C-centering operation, thus producing a staggering of the layers in the x direction.

Thompson (*43*) showed that the $(SiO_3)_2^{4-}$ chains in silicate pyroxenes have two distinct configurations with respect to the octahedral chains in the structure; a detailed examination of possible geometrical models for silicate pyroxenes later (*44*) revealed that three distinct configurations could be recognized. These are illustrated in Fig. 5. When the triangular faces (those approximately normal to a^*) of the tetrahedra are similarly directed to the triangular faces of the octahedral strip to which they are linked, the tetrahedral chain is designated as S rotated. When the triangular tetrahedral face is directed oppositely to the triangular faces of the octahedra, the tetrahedra is designated as O rotated. Thus complete S rotation (see Fig. 5b) results in hexagonal close packing of anions whereas complete O rotation results in cubic close packing of anions. In addition, a third variant may be recognized (Fig. 5c), the extended or E chain. Thus in terms of the O(3)–O(3)′–O(3)″ angle and the amount of O rotation, the O-rotated chain has O(3)–O(3)′–O(3)″ = 120° and an O rotation of 60°, the E chain has O(3)–O(3)′–O(3)″ = 180° and an O rotation of 0° and the S-rotated chain has O(3)–O(3)′–

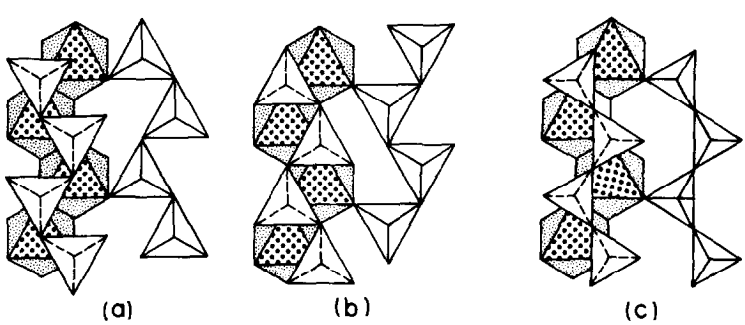

FIG. 5. Some geometrical stacking possibilities for pyroxenes structures, illustrating the three different chain configurations: (a) O-rotated chain; (b) S-rotated chain; (c) E (extended) chain.

O(3)'' = 240° and an O rotation of −60°. Although structures exhibiting nearly completely O-rotated chains do occur, for example $CoGeO_3$ (*51*), the vanadates and silicates discussed here correspond most closely to the E-chain model. However, many of these compounds exhibit partly rotated chains, and it is the direction and amount of this rotation that has been the subject of several recent studies (*43, 44*). In agreement with previous usage, chains with positive O rotations will be referred to as O-rotated chains irrespective of the amount of O rotation; it should be emphasized that this does not indicate that they correspond to the completely O-rotated model illustrated in Fig. 5a.

Examination of the alkali metal metavanadate structures (Figs. 3a, b, 4) shows that all types of chain configuration occurs in this group. $LiVO_3$ has an S-rotated chain, $NaVO_3$ has an O-rotated chain, and all the orthorhombic structures have E chains. Several explanations have been proposed for the various chain configurations in the silicate pyroxenes. Papike *et al.* (*44*) note that S rotation decreases the size of the $M(2)$ site whereas O rotation increases it, and they suggest that the Li pyroxenes spodumene ($LiAlSi_2O_6$) and $LiFeSi_2O_6$ show S rotations because Li requires a sixfold coordination whereas the sodic pyroxenes $NaM^{3+}Si_2O_6$ (M = Al, Fe^{3+}, Cr^{3+}, In) show O rotations because Na requires eightfold coordination. This cannot be considered as satisfactory for two reasons: $LiScSi_2O_6$ (*32*) shows an O-rotated tetrahedral chain with a Li coordination number of [6]; thus S rotations are not necessary for Li to achieve sixfold coordination. In addition, there is no reason for supposing that Na requires a coordination number of [8]; in $NaVO_3$ (*11*), Na(2) is in sixfold coordination and has an O-rotated chain. It can be shown (*32, 45*) that the displacement of the "back to back" chains in the pyroxene structure is the major factor controlling the coordination of the $M2$ site, and that this displacement is effected by an expansion and rotation of the O2–O2 edge of the $M1$ octahedron together with O rotation of the tetrahedral chain. These parameters have been calculated for the alkali pyroxenes and are shown in Table VIII. It is immediately apparent upon inspection of this table that those pyroxenes exhibiting a [6]-fold coordination of $M2$ are characterized by large chain displacements (1.44–1.93 Å) whereas those exhibiting an [8]-fold $M2$ coordination have smaller chain displacements (0.90–1.08 Å), irrespective of the identity of the $M2$ cation.

TABLE VIII

ROTATIONS AND DISPLACEMENTS IN THE ALKALI PYROXENES

	1 (Å)[c]	2(°)[b]	3(Å)[c]	4(°)[d]
$LiVO_3$	1.927	8.1	1.408	−18.2
$LiAlSi_2O_6$	1.535	4.8	1.410	−9.5
$LiFeSi_2O_6$	1.531	−0.3	1.721	0.0
$LiScSi_2O_6$	1.609	−3.3	1.892	4.4
$NaVO_3$	1.435	2.9	1.831	5.6
$NaAlSi_2O_6$	0.895	8.9	1.240	5.4
$NaFeSi_2O_6$	0.982	8.0	1.350	6.0
$NaScSi_2O_6$	1.063	6.9	1.433	6.4
$NaInSi_2O_6$	1.075	5.0	1.571	9.2

[a] Tetrahedral chain displacement = $2(cz_{O3} - a \cos\beta(0.5 - x_{O3}))$.

[b] O2–O2 rotation = $\sin^{-1}(2\, ax_{O2} \sin\beta/(O2\text{–}O2)) - 54.74°$.

[c] O2–O2 displacement along $Z = 2(c(z_{O2} - 0.25) - (0.5 - x_{O2})a \cos\beta)$.

[d] O–rotation = 180° − (O3–O3–O3). A negative value indicates an S rotation.

Figure 6 shows the variation in $\langle M2\text{–}O\rangle$ as a function of the ionic radius of the $M1$ cation in the alkali pyroxenes; a strong positive correlation is exhibited for both [6]- and [8]-fold coordination. Although this would suggest that the increase in the $\langle M2\text{–}O\rangle$ bond lengths (Table IX) is the result of the $M2$ cavity expanding because of the increase in size of the surrounding $M1$ octahedra, this would not appear to be satisfactory as the mean bond lengths may be adjusted by rotation and shear of the tetrahedra irrespective of the size of the $M1$ octahedra. There is no apparent explanation of the deviation in bond strength

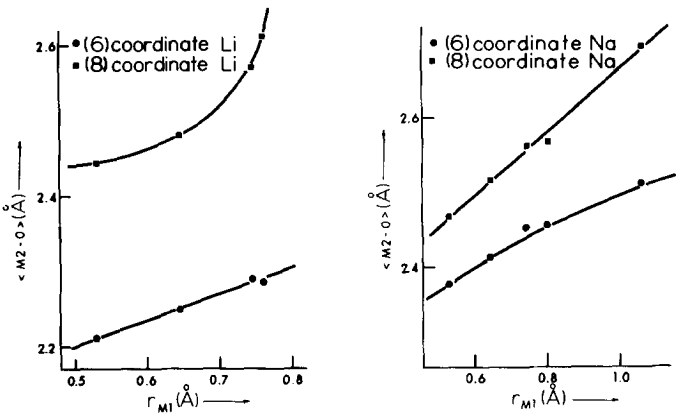

FIG. 6. The mean $M2$–O distance vs ionic radius of the $M1$ cation for the monoclinic pyroxenes $LiMX_2O_6$ (M = Al, Fe^{3+}, Sc, Li; X = Si, V^{5+}) and $NaMX_2O_6$ (M = Al, Fe^{3+}, Sc, In, Li; X = Si, V^{5+}) for different coordination numbers of the $M2$ cation.

sums around the $M2$ cation in the alkali pyroxenes. In this connection, examination of the environment of the O3 atom in the silicate pyroxenes shows that a bond strength model cannot be ideal if a specific bond length corresponds to a particular bond strength. Table X shows the O3 coordination in the silicate pyroxenes. For a given $M2$ cation, the O3 coordination remains the same across the series as the O3 anion is not bonded to the $M1$ cation. As the size of the $M1$ cation increases, each of the bond lengths involving the O3 anion increases. Thus, if a particular bond strength is associated with a particular bond length, the sums around the O3 anion cannot be ideal across the series.

It has been suggested (*14*) that the $M2$ cation in the pyroxene structures is positionally disordered, and that the poor bond strength sums arise as a result of constraining the $M2$ cation to occupy the special position at 4*e*. Numerous arguments can be marshaled for and against this proposal, but this question is at present inconclusive and low-temperature structural studies are needed to resolve this point.

The variation in cell dimensions with ionic radius of the alkali cation for the alkali metavanadates is shown in Fig. 7; in order that the dimensions may be compared directly between the orthorhombic and monoclinic structures, the variation in $a \sin \beta/2$ is shown for the monoclinic structures. As the c axis is controlled by the repeat distance of the tetrahedral chain, the geometrical changes of the chain in response to increasing alkali cation radius are of great interest. In the silicate pyroxenes, the principal mechanism of accommodation of the tetrahedral chain c-axis expansion is expansion of the Si–O3 bond lengths from 1.624 Å in $LiAlSi_2O_6$ to 1.688 Å in $CaMnSi_2O_6$. In contrast to this, the ⟨V–O3⟩ bond length is constant across the alkali metavanadate series

TABLE IX

⟨$M2$–O⟩ BOND LENGTHS[a] AND BOND STRENGTH SUMS FOR THE ALKALI PYROXENES

	⟨$M2$–O⟩^{VI}	⟨$M2$–O⟩^{VIII}	$\sum s_{M2-O}$
$LiAlSi_2O_6$	2.211	(2.445)	0.890
$LiFeSi_2O_6$	2.249	(2.481)	0.856
$LiScSi_2O_6$	2.289	(2.541)	0.852
$LiVO_3$	2.285	(2.581)	0.876
$NaAlSi_2O_6$	(2.378)	2.469	1.375
$NaFeSi_2O_6$	(2.414)	2.518	1.276
$NaScSi_2O_6$	(2.454)	2.564	1.184
$NaInSi_2O_6$	(2.457)	2.568	1.186
$NaVO_3$	2.513	(2.695)	0.928

[a] Values not in parentheses correspond to the generally accepted coordination number; the bond strength sum around $M2$ is for this coordination number.

TABLE X

O3–CATION DISTANCES IN THE ALKALI METASILICATE PYROXENES

*M*2	Li			Na			
*M*1	Al	Fe	Sc	Al	Fe	Sc	In
O3–Si	1.622	1.626	1.628	1.628	1.637	1.653	1.649
O3–Si	1.626	1.627	1.632	1.636	1.646	1.653	1.655
O3–*M*2	2.251	2.459	2.651	2.363	2.430	2.461	2.510
O3–*M*2	(3.144)	(3.178)	(3.299)	2.741	2.831	2.894	2.899

where differences of 0.2 Å in the *c*-axis occur. As shown in Fig. 8, the principal method of accommodation is by angular distortion of the vanadate tetrahedron. The similarity of the V–O bond lengths in the orthorhombic metavanadates would appear to result from the difference in interchain linkage between the monoclinic and orthorhombic structures. The increase in alkali cation coordination (from [6] in the monoclinic metavanadates to [8] or [10] in the orthorhombic metavanadates) is accompanied by an increase in anion coordination (see Table V); this produces a much greater flexibility in the structure, as evidenced by the incorporation of the NH_4^+ ion into the structure. The alkali metal cation is surrounded by eight anions between 2.73 and 3.15 Å (for KVO_3) with a further pair of anions at 3.41 Å. Bond strength tables (see Table XI) are slightly better for an alkali cation coordination number of [10]. The longest interaction is fairly weak but increases with increasing alkali cation radius and may be significant in $CsVO_3$; in this regard, in the structure of the Cs-rich beryl (*48*), Cs is surrounded by 12 oxygen anions at a distance of 3.43 Å, indicating that this is a reasonable Cs–O bonding distance.

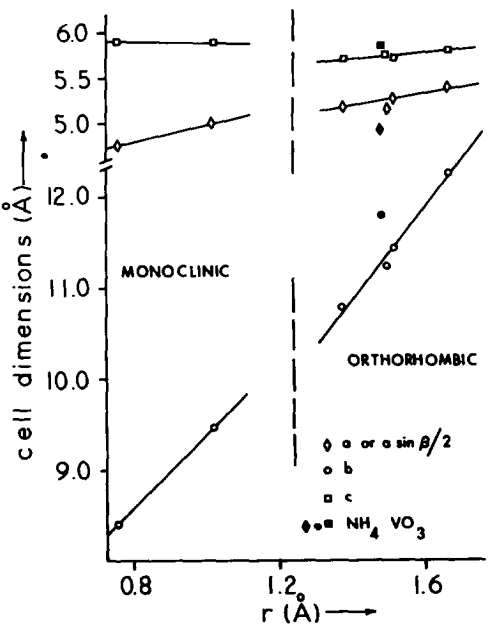

FIG. 7. The variation in cell dimensions with ionic radius of the alkali–metal cation in the metavanadates; for the orthorhombic structures, the coordination number was taken as [8], except for NH_4^- where [6] was used.

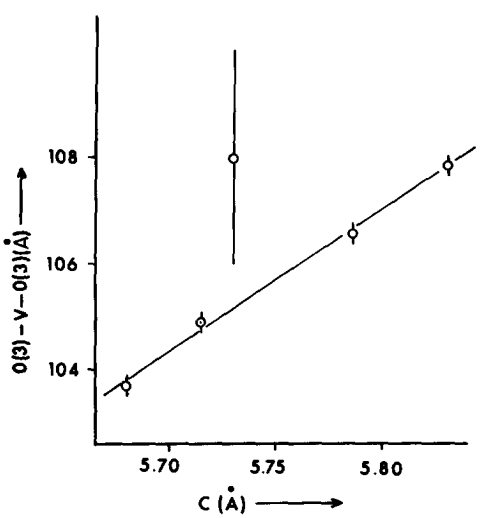

FIG. 8. The variation in the O–V–O angle as a function of the *c*-axis length in the alkali-metal metavanadates.

TABLE XI

EMPIRICAL BOND STRENGTH TABLES FOR SOME OF THE ALKALI METAL METAVANDATES[a]

$LiVO_3$

	Li(1)	Li(2)	V	Σ
O(1)	$0.18^{\times 2}_{\downarrow}$ $0.12^{\times 2}_{\downarrow}$	$0.22^{\times 2}_{\downarrow}$	1.46	1.98
O(2)	$0.23^{\times 2}_{\downarrow}$	$0.07^{\times 2}_{\downarrow}$	1.62	1.92
O(3)		$0.17^{\times 2}_{\downarrow}$	0.99 0.92	2.07
Σ	1.07	0.92	4.99	

$NaVO_3$

	Na(1)	Na(2)	V	Σ
O(1)	$0.19^{\times 2}_{\downarrow}$ $0.19^{\times 2}_{\downarrow}$	$0.18^{\times 2}_{\downarrow}$	1.50	2.06
O(2)	$0.23^{\times 2}_{\downarrow}$	$0.14^{\times 2}_{\downarrow}$	1.61	1.98
O(3)		$0.12^{\times 2}_{\downarrow}$	0.96 0.97	2.05
Σ	1.12	0.88	5.04	

KVO_3

	K	V	Σ[b]
O(1)	0.14 0.11 $0.08^{\times 2\rightarrow}_{\downarrow}$	1.55	1.96
O(2)	0.15 0.07 $(0.05^{\times 2\rightarrow}_{\downarrow})$	1.57	1.79(1.89)
O(3)	$0.14^{\times 2\rightarrow}_{\downarrow}$	$0.96^{\times 2\rightarrow}_{\downarrow}$	2.19
Σ	0.91(1.01)	5.04	

$RbVO_3$

	Rb	V	Σ[b]
O(1)	0.14 0.10 $0.09^{\times 2\rightarrow}_{\downarrow}$	1.58	2.00
O(2)	0.13 0.08 $(0.06^{\times 2\rightarrow}_{\downarrow})$	1.64	1.85(1.97)
O(3)	$0.14^{\times 2\rightarrow}_{\downarrow}$	$0.97^{\times 2\rightarrow}_{\downarrow}$	2.22
Σ	0.91(1.03)	5.16	

$CsVO_3$

	Cs	V	Σ[b]
O(1)	0.15 0.11 $0.12^{\times 2\rightarrow}_{\downarrow}$	1.60	2.09
O(2)	0.12 0.10 $(0.08^{\times 2\rightarrow}_{\downarrow})$	1.57	1.78(1.94)
O(3)	$0.16^{\times 2\rightarrow}_{\downarrow}$	$0.96^{\times 2\rightarrow}_{\downarrow}$	2.24
Σ	1.02(1.18)	5.09	

[a] Calculated from the curves of Brown and Shannon (*46*) and Wu (*47*).

[b] Sums calculated for an alkali metal coordination number of [8]; values in parentheses calculated for alkali metal coordination number of [10].

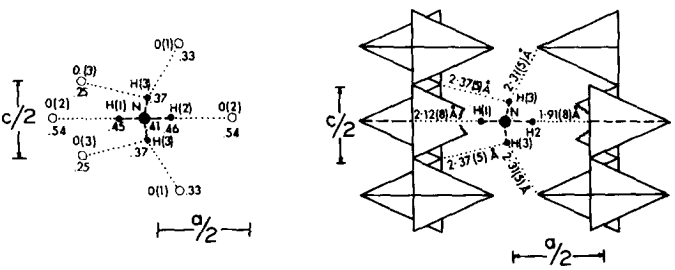

(a) (b)

FIG. 9. The structure of NH_4VO_3 in the vicinity of the NH_4 position, projected along the *b* axis: (a) the hydrogen bonding arrangement; donor–hydrogen bonds are indicated by the broken lines, and hydrogen–acceptor bonds are indicated by the dotted lines; (b) linkage of adjacent chains, showing the hydrogen–acceptor bond lengths involved in this linkage.

The environment of the NH_4^+ ion in NH_4VO_3 is given in Table VI and is illustrated in Fig. 9. Despite the fact that the hydrogen atoms are affected by systematic error due to delocalization of electron density along the N–H bond, the geometry of the NH_4^+ ion corresponds well with that exhibited in structures examined by neutron diffraction. As shown in Fig. 9, the NH_4^+ ion forms two single and two bifurcated hydrogen bonds with the surrounding anions. The acceptor anions are not the six shortest (NH_4^+)–O distances; the O(1)*b* and O(1)*c* approaches of 3.04 and 3.02 Å are considerably shorter than the observed donor acceptor distances of 3.22 Å to O(1)*d*. It is apparent that the acceptor anion configuration is controlled by the requirement that the NH_4^+ ion be approximately tetrahedral. As indicated in Fig. 7, the individual cell dimensions for NH_4VO_3 are not linear with the variation of the other alkali metavanadates despite the fact that the cell volume is linear on a type I stability diagram (see Fig. 2). Examination of Fig. 9 shows that the two O(2) anions involved in hydrogen bonding to the NH_4^+ ion are separated by one cell translation in the *x* direction. In order that these anions be within the range of hydrogen bonding of the NH_4^+ ion, the *a* dimension must be contracted with respect to that expected from a "cation" the size of the NH_4^+ ion (*50*), while in order for the cell volume to reflect the isostructural nature of the alkali metal metavanadates, the other two cell dimensions expand.

Acknowledgments

We would like to thank R. Faggiani, R. Morrow, and G. Ozog of the Materials Research Institute, McMaster University for their assistance during crystal preparation and data collection. Financial support was provided by the National Research Council of Canada and the University of Manitoba.

References

1. B. E. WARREN AND W. L. BRAGG, *Z. Kristallogr.* **69**, 168 (1928).
2. J. ZUSSMAN, *Earth Sci. Rev.* **4**, 39 (1968).
3. Pyroxenes and amphiboles: Crystal chemistry and phase petrology, *Mineral. Soc. Amer. Spec. Pap.* **2**, (1969).
4. R. D. SHANNON, *Chem. Comm.* 881 (1971).
5. R. D. SHANNON AND C. CALVO, *J. Solid State Chem.* **6**, 538 (1973).
6. I. D. BROWN AND R. D. SHANNON, *Acta Crystallogr. A* **29**, 266 (1973).
7. R. GOPAL AND C. CALVO, *Can. J. Chem.* **51**, 1004 (1973).
8. H. SØRUM, *Kgl. Norske Vidensk. Selsk. Forh.* **16**, 39 (1943).
9. R. S. FEIGELSON, G. W. MARTIN, AND B. C. JOHNSON, *J. Cryst. Growth* **13/14**, 686 (1972).
10. C. T. PREWITT, A. SACROUG, S. SUENO, AND M. CAMERON, *in* "Geol. Soc. Amer. Ann. Meet. Prog.," p. 630 (1972).
11. F. MARUMO, M. ISOBE, AND S. IWAI, *Acta Crystallogr. B* **30**, 1628 (1974).

12. P. K. BURKERT AND H. P. FRITZ, *Z. Naturforsch. B* **25**, 1053 (1970).
13. O. MULLER AND R. ROY, "The Major Ternary Structural Families," Springer-Verlag, Berlin (1974).
14. R. D. SHANNON AND C. CALVO, *Can. J. Chem.* **51**, 265 (1973).
15. R. SWANSON, G. W. MARTIN, AND R. S. FEIGELSON, *J. Cryst. Growth* **20**, 306 (1973).
16. J. S. LUKESH, *Acta Crystallogr.* **3**, 476 (1950).
17. J. S. LUKESH, *in* "Program and Abstracts," Amer. Cryst. Ass. Meet. Feb. 15–17, Vol. 21 (1951).
18. M. PETRASOVA, J. MADAR, AND F. HANIC, *Chem. Zvesti* **12**, 410 (1958).
19. H. T. EVANS AND S. BLOCK, *Amer. Mineral.* **39**, 326 (1954).
20. M. PETRASOVA, J. MADAR, AND F. HANIC, *Chem. Zvesti* **12**, 410 (1958).
21. H. T. EVANS, *Z. Kristallogr.* **114**, 257 (1960).
22. C. CALVO, *in* "Program and Abstracts," Amer. Cryst. Ass. Meet. June 23–27, Vol. 18 (1958).
23. M. GANNE AND M. TOURNOUX, *C.R. Acad. Sci. Paris Ser. C* **272**, 1858 (1971).
24. M. GANNE, Y. PIFFARD, AND M. TOURNOUX, *Can. J. Chem.* **52**, 3539 (1974).
25. H. D. MEGAW, *Acta Crystallogr.* **9**, 56 (1956).
26. C. W. BURNHAM, J. R. CLARK, J. J. PAPIKE, AND C. T. PREWITT, *Z. Kristallogr.* **125**, 1 (1967).
27. C. T. PREWITT AND C. W. BURNHAM, *Amer. Mineral.* **51**, 956 (1966).
28. D. E. APPLEMAN AND D. B. STEWART, *in* "Geol. Soc. Amer. Ann. Meet. Prog., San Francisco, California," p. 5 (1966).
29. J. R. CLARK, D. E. APPLEMAN, AND J. J. PAPIKE, *Mineral. Soc. Amer. Spec. Pap.* **2**, 31 (1969).
30. F. C. HAWTHORNE AND H. D. GRUNDY, *Acta Crystallogr. B* **29**, 2615 (1973).
31. F. C. HAWTHORNE AND H. D. GRUNDY, *Acta Crystallogr. B* **30**, 1882 (1974).
32. F. C. HAWTHORNE AND H. D. GRUNDY, *Can. Mineral.* **15**, 50 (1977).
33. J. S. STEPHENS, personal communication.
34. L. W. FINGER, personal communication.
35. D. T. CROMER AND J. B. MANN, *Acta Crystallogr.* **24**, 321 (1968).
36. D. T. CROMER AND D. LIBERMAN, *J. Chem. Phys.* **53**, 1891 (1970).
37. $R(\%) = \sum(|F_0| - |F_c|)/\sum|F_0|$; $R_w(\%) = (\sum w(|F_0| - |F_c|)^2/\sum wF_0^2)^{1/2}$, $w = 1$.
38. W. H. ZACHARIASEN, *Acta Crystallogr.* **23**, 558 (1967).
39. W. C. HAMILTON, *Acta Crystallogr.* **18**, 502 (1965).
40. R. D. SHANNON AND C. T. PREWITT, *J. Inorg. Nucl. Chem.* **32**, 1427 (1970).
41. Ionic radii were taken from R. D. SHANNON, *Acta Crystallogr. A* **32**, 751 (1976).
42. J. PERRAUD, *Rev. Chim. Miner.* **11**, 302 (1974).
43. J. B. THOMPSON. *Amer. Mineral.* **55**, 292 (1970).
44. J. J. PAPIKE, C. T. PREWITT, S. SUENO, AND M. CAMERON. *Z. Kristallogr.* **138**, 254 (1973).
45. M. CAMERON, S. SUENO, C. T. PREWITT, AND J. J. PAPIKE, *Amer. Mineral.* **58**, 594 (1973).
46. I. D. BROWN AND R. D. SHANNON, *Acta Crystallogr. A* **29**, 266 (1973).
47. I. D. BROWN AND K. K. WU, *Acta Crystallogr. B* **32**, 1957 (1976).
48. F. C. HAWTHORNE AND P. CERNY, *Can. Mineral.*, in press.
49. L. IDLER, personal communication.
50. A. A. KHAN AND W. H. BAUR, *Acta Crystallogr. B* **28**, 683 (1972).
51. D. R. PEACOR, *Z. Kristallogr.* **126**, 299 (1968).